Supporting information

Tailoring the room-temperature miscibility gap in ordered spinel $LiNi_{0.5}Mn_{1.5}O_4$ cathodes by multi-element doping

Shunsuke Narumi[‡a], Eugenio H. Otal[‡,a], Tien Quang Nguyen[‡,b], Michihisa Koyama[c], and Nobuyuki Zettsu[* a,b,c,d]

[a] Department of Materials Chemistry, Faculty of Engineering, Shinshu University, 4-17-1 Wakasato, Nagano 380-8553, Japan

[b] Institute for Aqua Regeneration, Shinshu University, 4-17-1 Wakasato, Nagano 380-8553, Japan

[c] Research Initiative for Supra-Materials, Shinshu University, 4-17-1 Wakasato, Nagano 380-8553, Japan

[d] Energy Landscape Architectonics Brain Bank, Shinshu University, 4-17-1 Wakasato, Nagano 380-8553, Japan

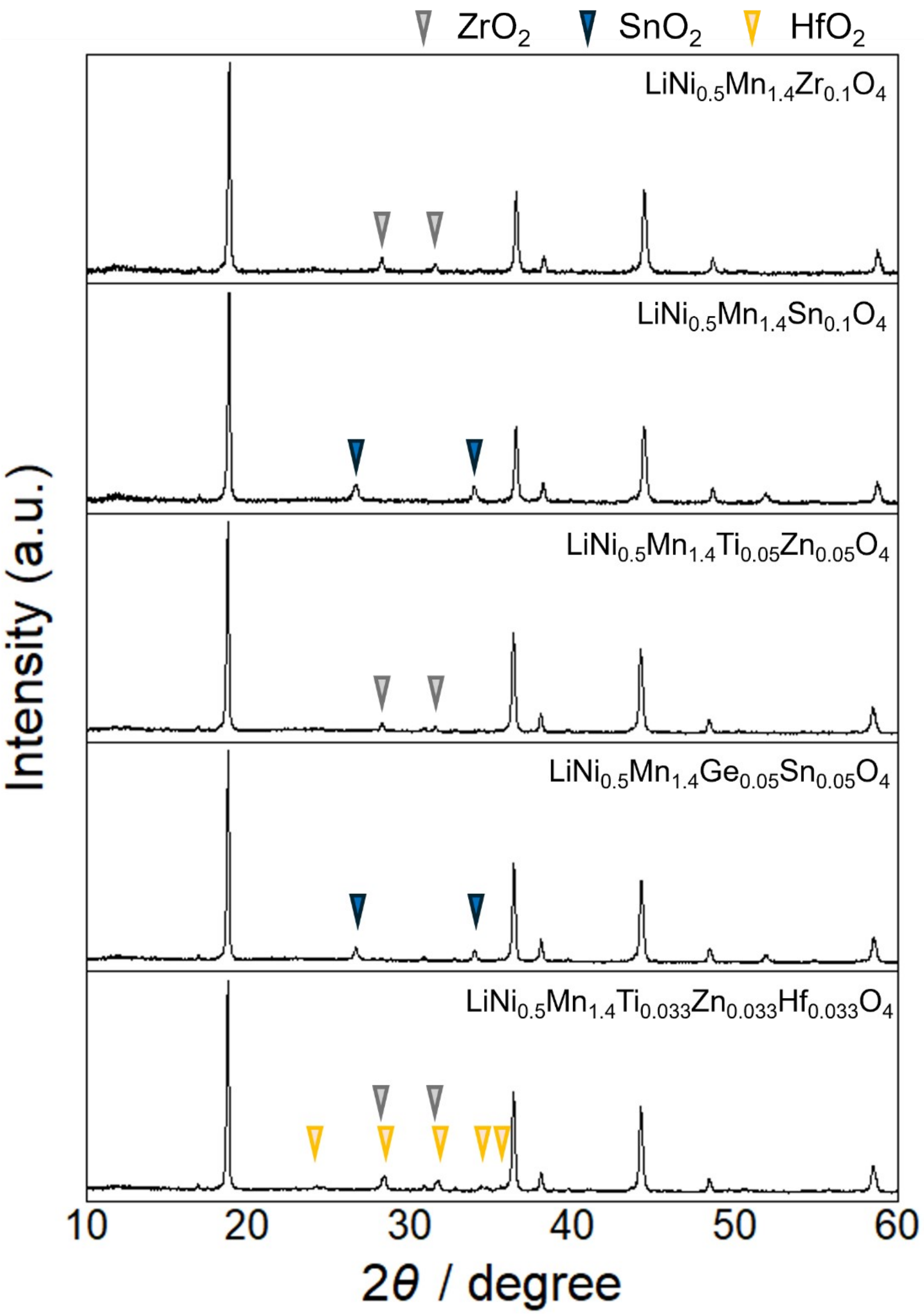

Fig. S1. PXRD patterns of LNMO substituted with Zr, Sn, and Hf.

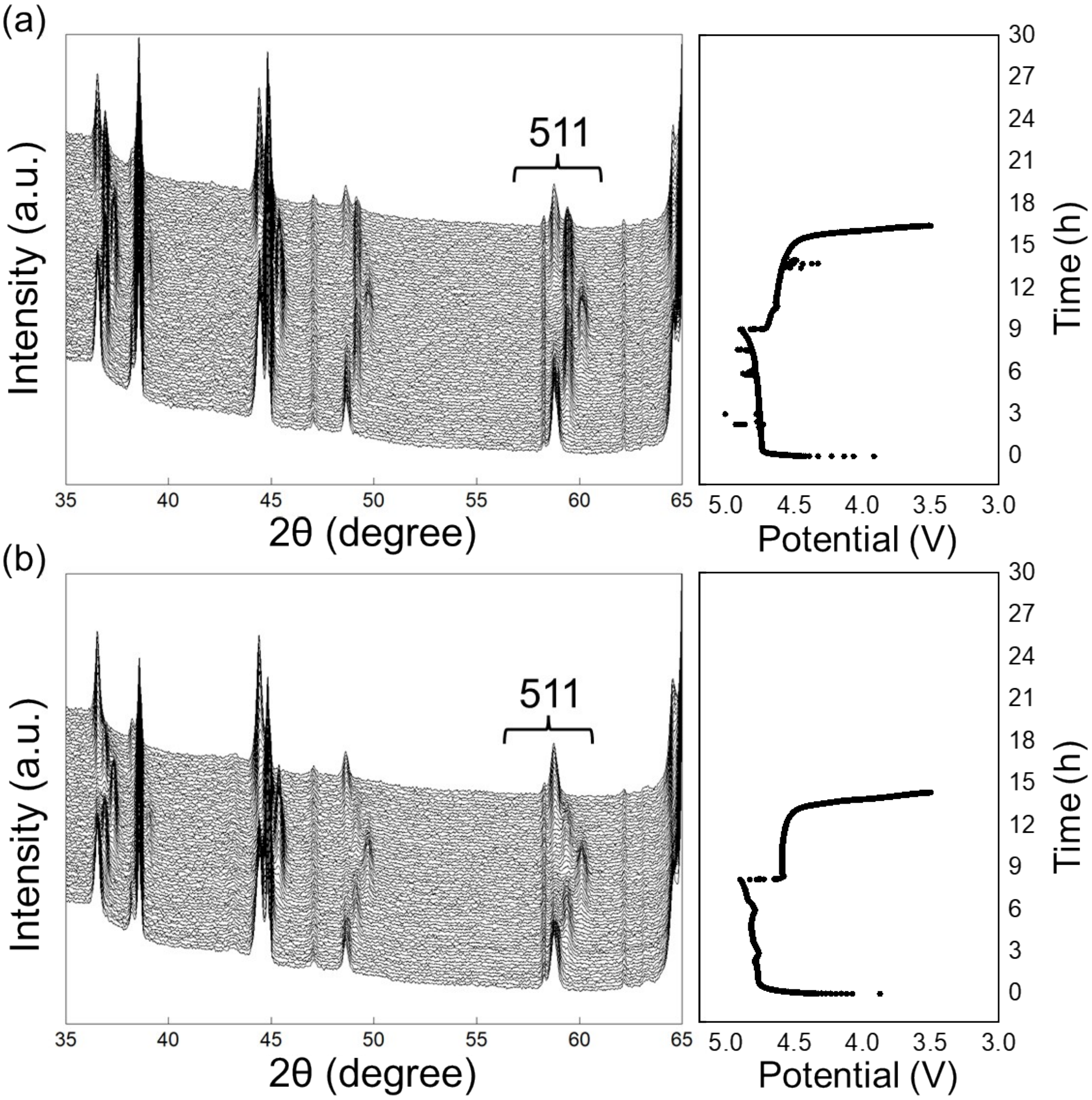

Fig. S2. *Operando* XRD data of LNMO (a) and STG-LNMO (b) electrodes-based coin-cell upon electrochemical charging and discharging process alongside corresponding electrochemical curves.

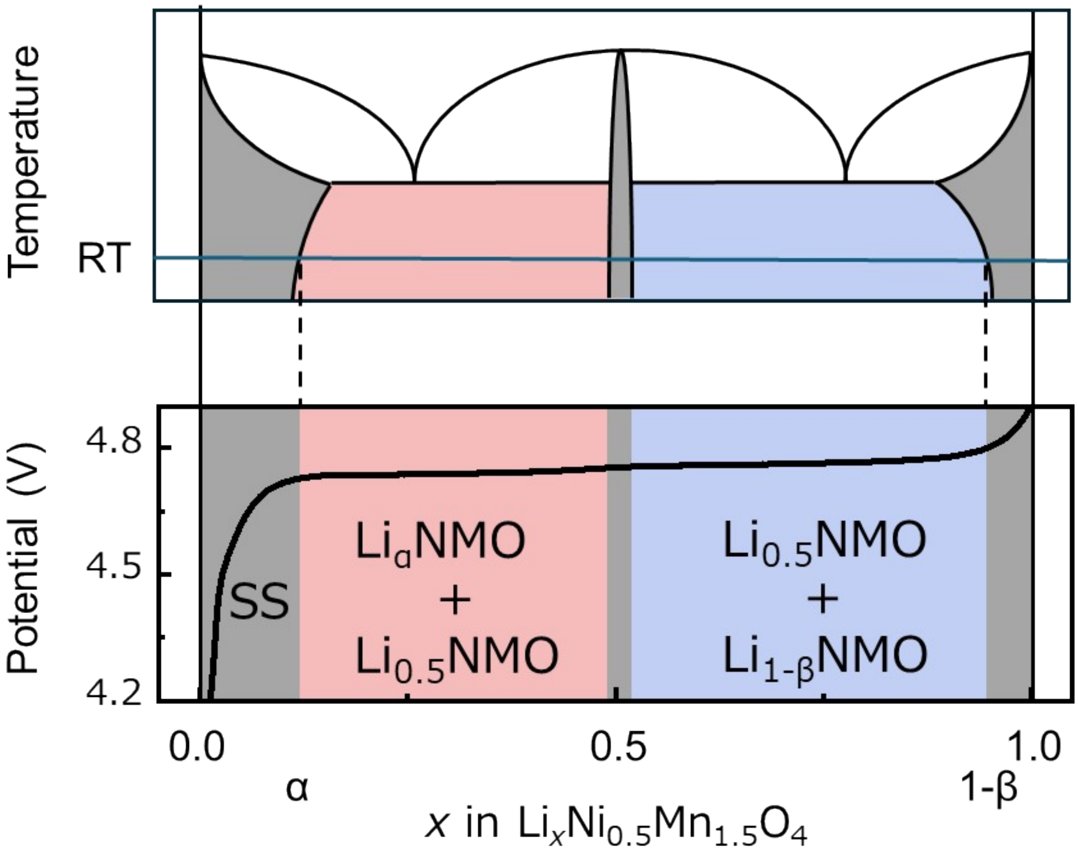

Fig. S3. Temperature–composition diagram of LNMO and miscibility gap (grey region) and solid solution domain (red and blue region) at room temperature.

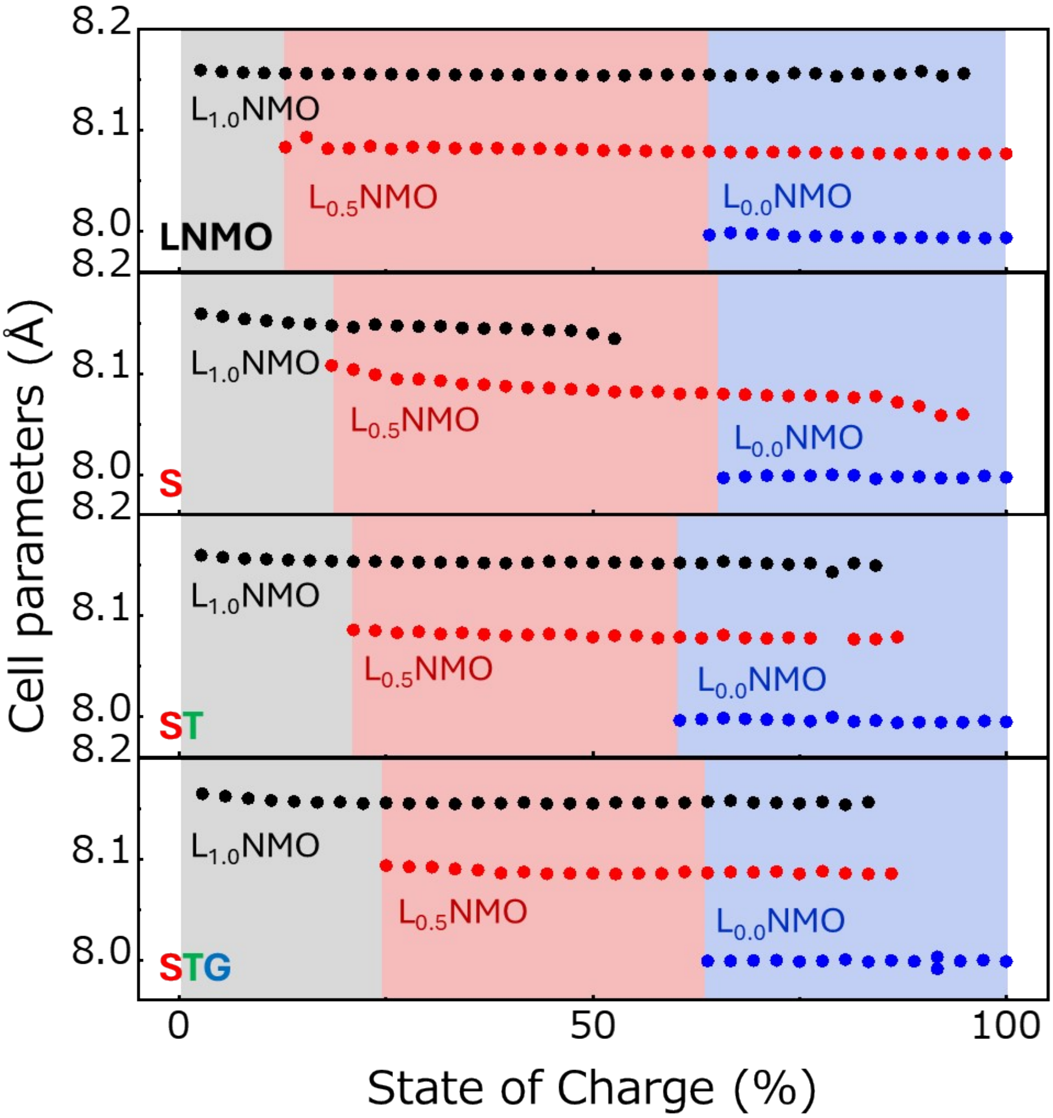

Fig. S4. The evolution of the lattice constant in LNMO, S-LNMO, ST-LNMO, and STG-LNMO as a function of SOC, determined from the 511 reflection in *operando* XRD measurements.

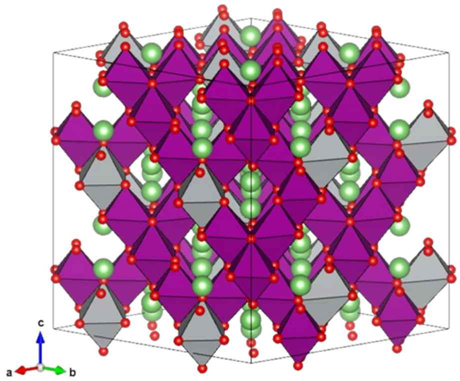

- **Space group: $P4_{3}32$** (no. 212)
- **Wyckoff positions:**

Li: 8c (T-site)	$(0+\delta, 0+\delta, 0+\delta)$
Ni: 4a (O-site)	$(5/8, 5/8, 5/8)$
Mn: 12d (O-site)	$(1/8, 3/8+\delta, 7/8+\delta)$
O: 8c and 24e	

- Supercell **(2×2×2)**: 448 atoms

Fig. S5. Supercell structure of ordered LNMO used in simulation and the Wyckoff positions of all atoms. Li and O atoms are presented in green and red spheres, respectively. While Ni and Mn are displayed by magenta and silver polyhedrons, respectively.

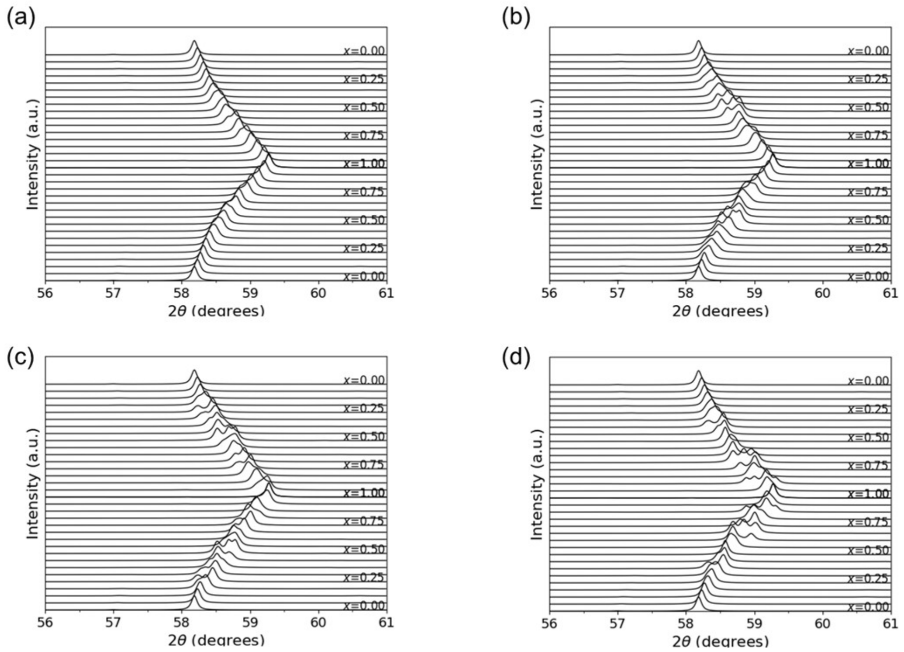

Fig. S6. Calculated XRD profiles of LNMO with *2θ* ranging from 56 to 61 degrees (511 reflection) as a function of delithiation level *x* for various Li deintercalation scenarios: (a) scenario 1, (b) scenario 2, (c) scenario 3, and (d) scenarios 4, respectively.

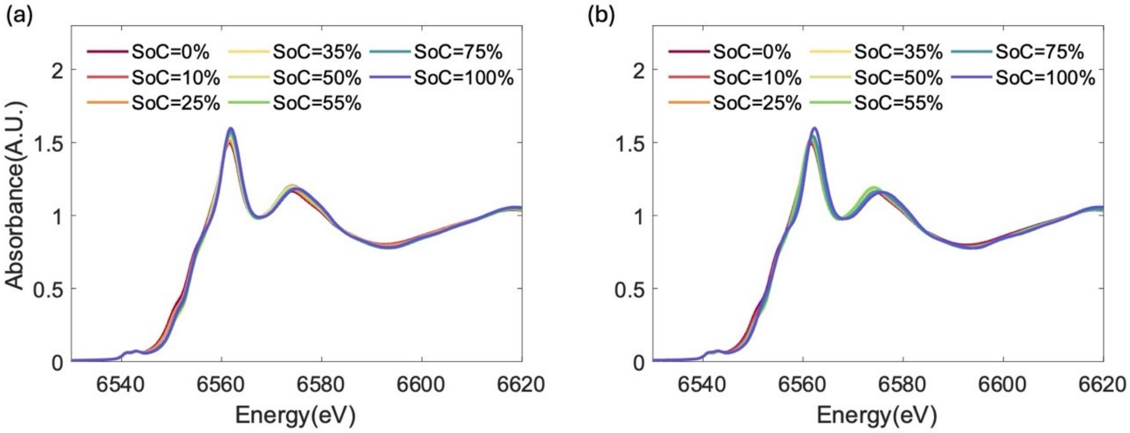

Fig. S7. *Ex-situ* XANES measurements of Mn K edge to SOC-controlled (a) LNMO and (b) STG-LNMO electrodes.

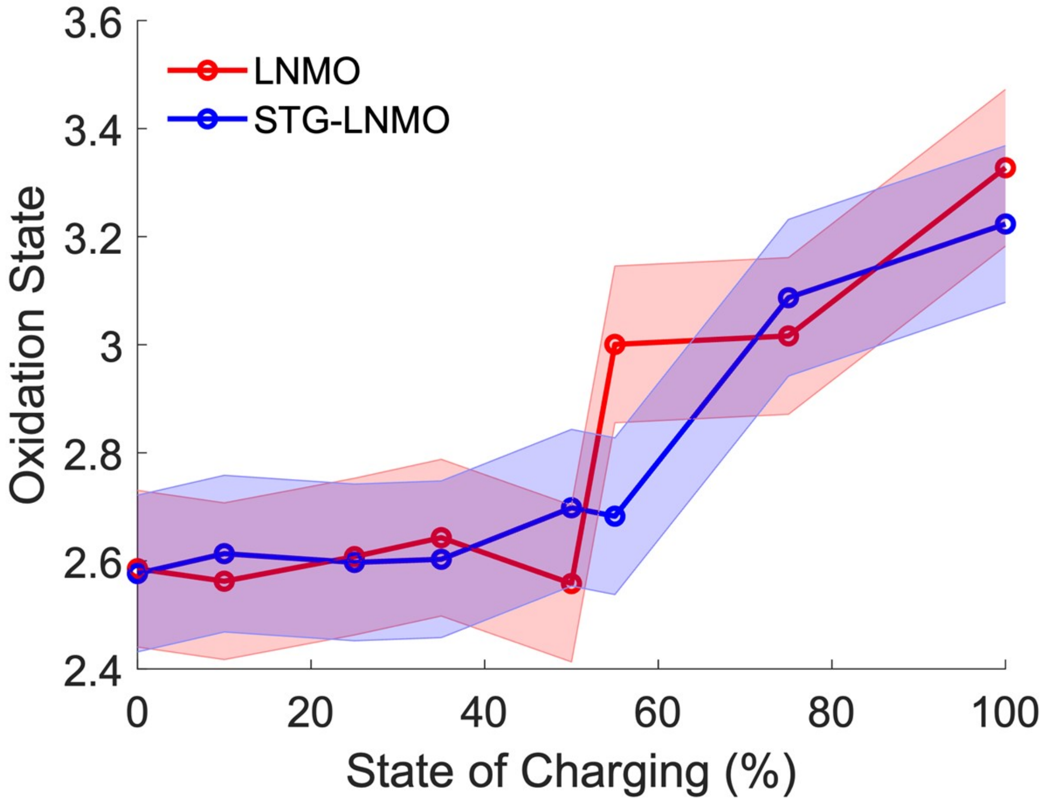

Fig. S8. Evolution of oxidation states of Ni upon electrochemical charging process of LNMO and STG-LNMO.

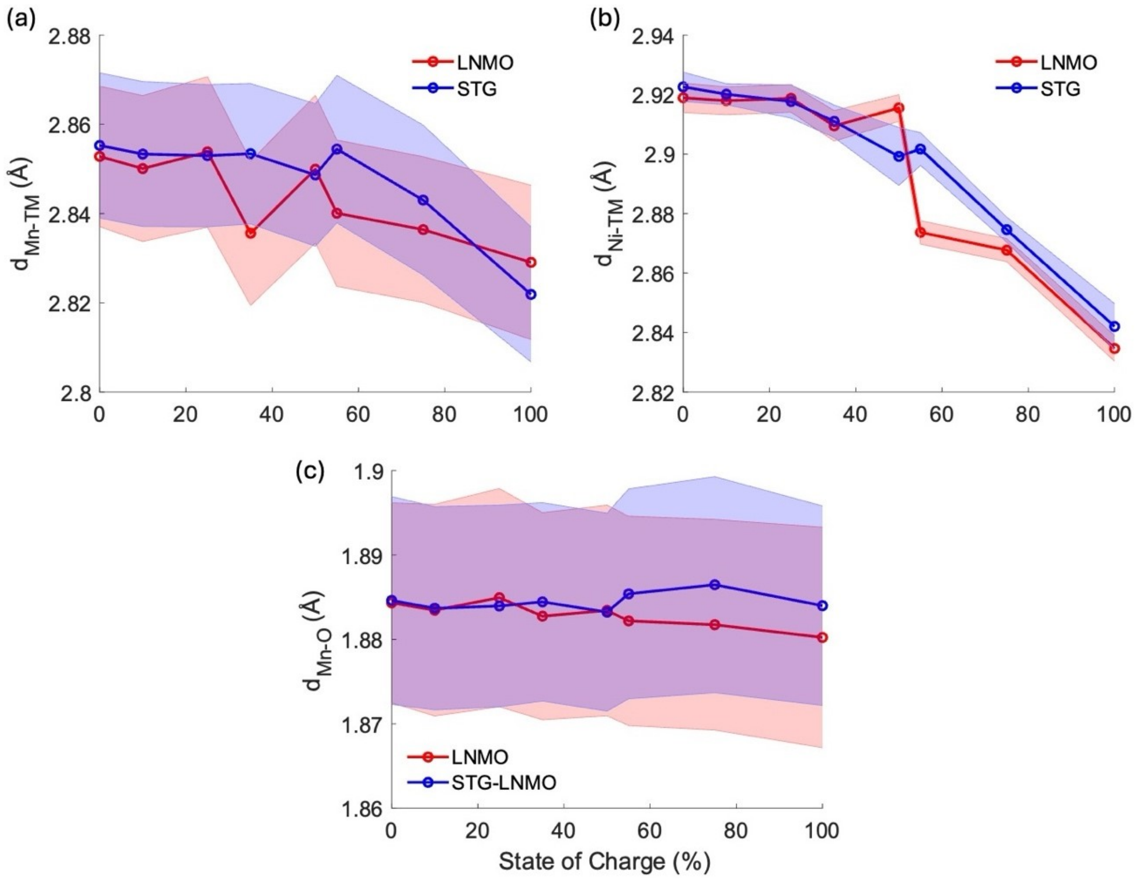

Fig. S9. Evolution of bond lengths of (a) Mn and (b) Ni to their second coordination shells, and (c) the evolution of bond length of closest Mn−next neighbor shells (Mn−O) upon electrochemical charging process of LNMO and STG-LNMO.

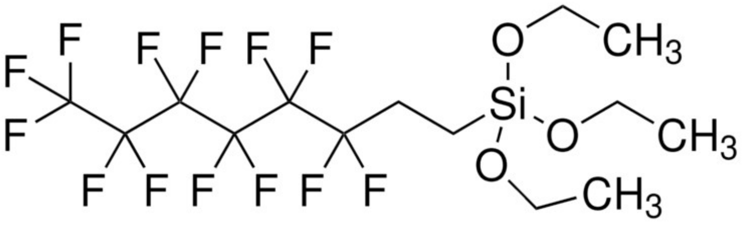

Fig. S10. Chemical structure of 1H,1H,2H,2H-perfluorooctyltriethoxysilane, $F_3C(CF_2)_5(CH2)_2Si(OCH_3)_3$.

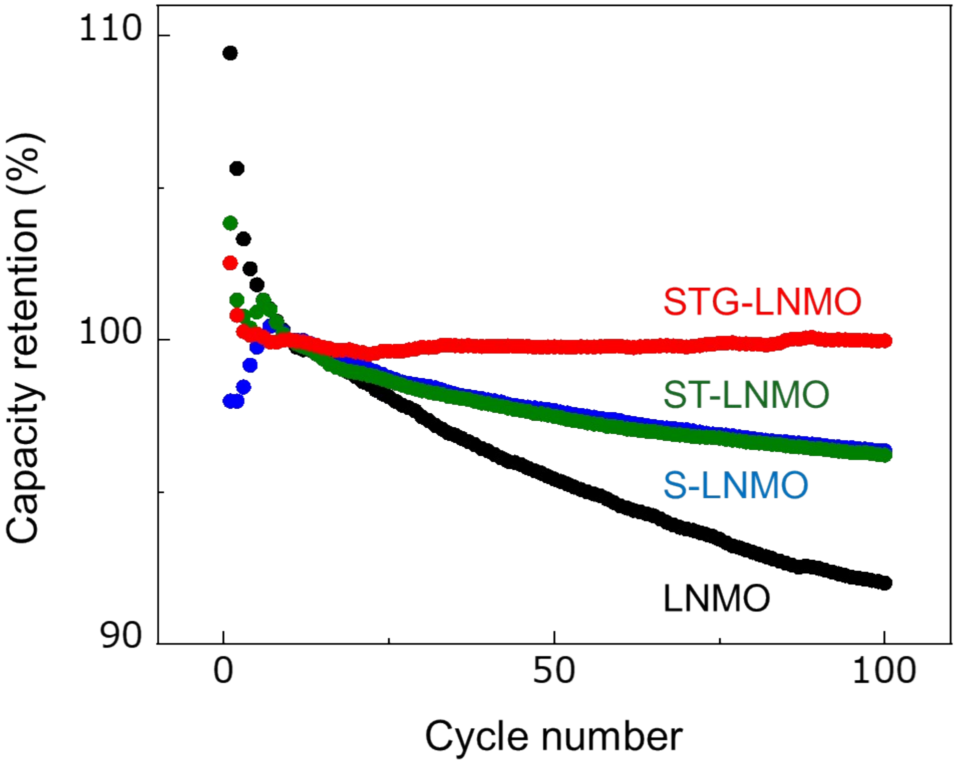

Fig. S11. Cycling performance tests of LNMO, S-LNMO, ST-LNMO and STG-LNMO based half-cells at 0.5C charge and 1C discharge, with operating voltage range of 3.5-4.9 V (vs. Li/Li^+), recorded at room temperature.

Table S1. Stoichiometry of the LNMO and STG-LNMO compounds determined by ICP-OES.

	Li	Ni	Mn	Si	Ti	Ge
LNMO	0.939	0.500	1.528			
STG-LNMO	0.990	0.500	1.390	0.036	0.034	0.026

Table S2. Refined crystallographic parameters of LNMO derivatives based on XRD results.

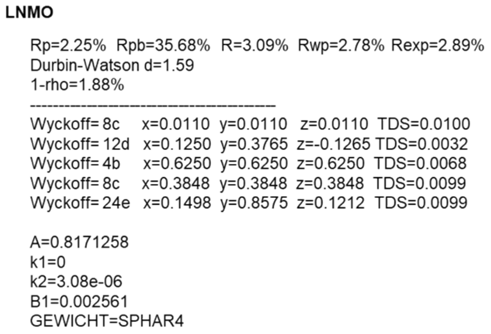

LNMO

```
Rp=2.25%  Rpb=35.68%  R=3.09%  Rwp=2.78%  Rexp=2.89%
Durbin-Watson d=1.59
1-rho=1.88%
-----------------------------------
Wyckoff= 8c     x=0.0110  y=0.0110   z=0.0110  TDS=0.0100
Wyckoff= 12d   x=0.1250  y=0.3765  z=-0.1265 TDS=0.0032
Wyckoff= 4b     x=0.6250  y=0.6250  z=0.6250  TDS=0.0068
Wyckoff= 8c     x=0.3848  y=0.3848  z=0.3848  TDS=0.0099
Wyckoff= 24e   x=0.1498  y=0.8575  z=0.1212  TDS=0.0099

A=0.8171258
k1=0
k2=3.08e-06
B1=0.002561
GEWICHT=SPHAR4
```

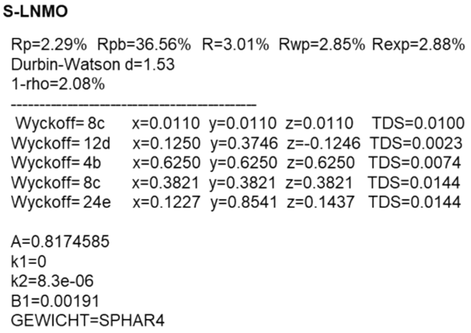

S-LNMO

```
Rp=2.29%  Rpb=36.56%  R=3.01%  Rwp=2.85%  Rexp=2.88%
Durbin-Watson d=1.53
1-rho=2.08%
-----------------------------------
 Wyckoff= 8c       x=0.0110  y=0.0110  z=0.0110    TDS=0.0100
Wyckoff= 12d     x=0.1250  y=0.3746  z=-0.1246  TDS=0.0023
Wyckoff= 4b       x=0.6250  y=0.6250  z=0.6250   TDS=0.0074
Wyckoff= 8c       x=0.3821  y=0.3821  z=0.3821   TDS=0.0144
Wyckoff= 24e     x=0.1227  y=0.8541  z=0.1437   TDS=0.0144

A=0.8174585
k1=0
k2=8.3e-06
B1=0.00191
GEWICHT=SPHAR4
```

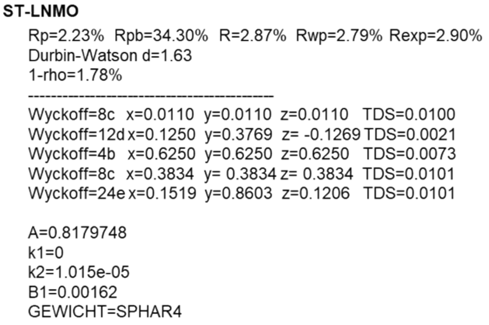

ST-LNMO

```
Rp=2.23%  Rpb=34.30%  R=2.87%  Rwp=2.79%  Rexp=2.90%
Durbin-Watson d=1.63
1-rho=1.78%
-----------------------------------
Wyckoff=8c   x=0.0110  y=0.0110  z=0.0110   TDS=0.0100
Wyckoff=12d x=0.1250  y=0.3769  z= -0.1269 TDS=0.0021
Wyckoff=4b   x=0.6250  y=0.6250  z=0.6250   TDS=0.0073
Wyckoff=8c   x=0.3834  y= 0.3834 z= 0.3834  TDS=0.0101
Wyckoff=24e x=0.1519  y=0.8603  z=0.1206   TDS=0.0101

A=0.8179748
k1=0
k2=1.015e-05
B1=0.00162
GEWICHT=SPHAR4
```

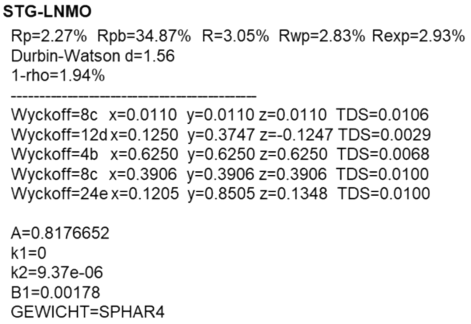

STG-LNMO

```
Rp=2.27%  Rpb=34.87%  R=3.05%  Rwp=2.83%  Rexp=2.93%
Durbin-Watson d=1.56
1-rho=1.94%
-----------------------------------
Wyckoff=8c   x=0.0110  y=0.0110 z=0.0110  TDS=0.0106
Wyckoff=12d x=0.1250  y=0.3747 z=-0.1247 TDS=0.0029
Wyckoff=4b   x=0.6250  y=0.6250 z=0.6250  TDS=0.0068
Wyckoff=8c   x=0.3906  y=0.3906 z=0.3906  TDS=0.0100
Wyckoff=24e x=0.1205  y=0.8505 z=0.1348  TDS=0.0100

A=0.8176652
k1=0
k2=9.37e-06
B1=0.00178
GEWICHT=SPHAR4
```

Table S3. Substitutional energies (in eV) for replacing Ni or Mn with Si, Ge, or Ti in ordered LNMO. Lower substitutional energy indicates a stronger preference for the dopant to occupy a specific site.

Structure	ΔE_{DFT}		ΔE_{PFP}	
	With U	Without U	With U	Without U
LNMO_Si@Mn	**0.701**	**0.722**	**0.663**	**0.710**
LNMO_Si@Ni	2.006	3.223	1.764	2.841
LNMO_Ge@Mn	**0.073**	**-0.129**	**0.048**	**0.100**
LNMO_Ge@Ni	1.323	3.158	1.108	2.102
LNMO_Ti@Mn	**0.517**	**0.367**	**0.520**	**0.521**
LNMO_Ti@Ni	1.726	2.875	1.560	3.496

Table S4. Values for bonding distances and coordination numbers (C.N.) obtained from EXAFS fitting.

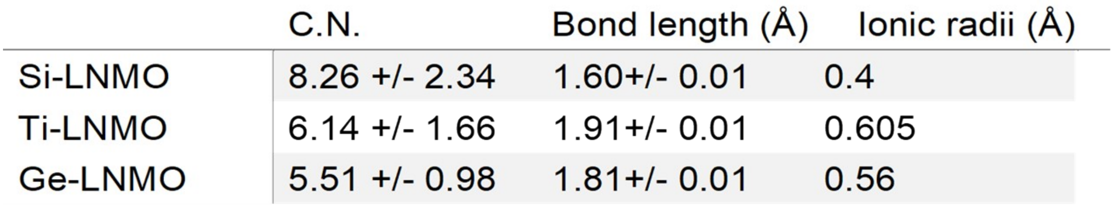

	C.N.	Bond length (Å)	Ionic radii (Å)
Si-LNMO	8.26 +/- 2.34	1.60+/- 0.01	0.4
Ti-LNMO	6.14 +/- 1.66	1.91+/- 0.01	0.605
Ge-LNMO	5.51 +/- 0.98	1.81+/- 0.01	0.56

Table S5. The peak intensity ratio of I_{580}/I_{620} in FT-IR spectra taken from the LNMO derivatives. Disordered LNMO (*Fd*-3*m*) was synthesized by solid state synthesis. Stoichiometric mixture of starting materials (1.05 times excess to compensate of Li loss at high temperature) was placed in 30 cm^3 crucibles. The mixed powders were directly calcined at 800 °C for 10 h in Muffle furnace under air atmosphere with heating rate of 700 °C·h-1 and cooled down to 500 °C with cooling rate of 200 °C·h^{-1}.

Sample	I_{580}/I_{620}	Sample	I_{580}/I_{620}
LNMO($P4_332$)	1.08	S-LNMO	1.04
LNMO(*F*d-3m)	0.86	S,T-LNMO	1.01
		STG-LNMO	1.06

Table S6. Typical discharge capacity of LNMO derivatives-based half-cells.

Sample	Discharge capacity (mAh·g^{-1})
LNMO	130.0
S-LNMO	119.6
ST-LNMO	131.3
STG-LNMO	124.2

The theoretical specific capacities for LNMO, S-LNMO, ST-LNMO, and STG-LNMO are 146.7 mAh/g, 148.9 mAh/g, 148.1 mAh/g, and 147.1 mAh/g, respectively. Since ST-LNMO exhibited a higher theoretical specific capacity than STG-LNMO, this could partly explain the higher discharge capacity observed for ST-LNMO. Therefore, while multi-element substitution influences the system's configurational entropy, it does not necessarily improve discharge capacity in a straightforward manner.

Table S7. Discharge capacity retention rates of LNMO, S-LNMO, ST-LNMO and STG-LNMO between the 10th and 100th cycles.

sample	Retention rate (%)
LNMO	92.0
S-LNMO	96.3
ST-LNMO	96.2
STG-LNMO	99.9